A hydrocarbon reaction model for low temperature hydrogen plasmas and an application to the Joint European Torus

D. A. Alman and D. N. Ruzic
Department of Nuclear, Plasma, and Radiological Engineering, University of Illinois, Urbana, Illinois 61801

J. N. Brooks
Argonne National Laboratory, Argonne, Illinois 60439

(Received 4 May 1999; accepted 22 December 1999)

A model of collisional processes of hydrocarbons in hydrogen plasmas has been developed to aid in computer modeling efforts relevant to plasma–surface interactions. It includes 16 molecules (CH up to CH_4, C_2H to C_2H_6, and C_3H to C_3H_6) and four reaction types (electron impact ionization/dissociative ionization, electron impact dissociation, proton impact charge exchange, and dissociative recombination). Experimental reaction rates or cross sections have been compiled, and estimates have been made for cases where these are not available. The proton impact charge exchange reaction rates are calculated from a theoretical model using molecular polarizabilities. Dissociative recombination rates are described by the equation A/T^B where parameter A is fit using polarizabilities and B is estimated from known reaction rates. The electron impact ionization and dissociation cross sections are fit to known graphs using four parameters: threshold energy, maximum value of the cross section, energy at the maximum, and a constant for the exponential decay as energy increases. The model has recently been used in an analysis of the Joint European Torus [P. H. Rebut, R. J. Bickerton, and B. E. Keen, Nucl. Fusion **25**, 1011 (1985)] MARK II carbon inner divertor using the WBC Monte Carlo impurity transport code. The updated version of WBC, which includes the full set of hydrocarbon reactions, helps to explain an observed asymmetry in carbon deposition near the divertor. © *2000 American Institute of Physics.* [S1070-664X(00)00505-X]

I. INTRODUCTION

Graphite tiles are commonly used as plasma facing components in fusion devices. The advantages of using carbon are its capability of withstanding high heat fluxes without its structure being degraded and its low atomic number that keeps radiation losses from the core plasma to a minimum. However, carbon is problematic since it is susceptible to chemical sputtering in the presence of a hydrogen plasma. The result is the release of various hydrocarbon impurities into the plasma. These hydrocarbons are dominated by methane, but have been shown to contain significant amounts of heavier hydrocarbons, i.e., C_2H_x and C_3H_x species. These heavier hydrocarbons can account for up to 50% of the total erosion of graphite under hydrogen impact.[1] In the course of computer modeling efforts, the need for detailed information concerning gas phase reactions between these hydrocarbons and the background hydrogen plasma has arisen. While there have been previous attempts to provide such information,[2] there is no source for the complete set of cross sections and/or rate coefficients for methane and higher hydrocarbons. Hence, there is an urgent need for this sort of systematic data over a wide range of collision energies, with uncertainties on the order of a factor of 2 or more being acceptable.[1] Additionally, new experimental data have been published since earlier efforts.[3–6] The goal here is to fill in these troublesome gaps in the knowledge base with reasonable approximations that will allow improved computer modeling. Additional work is being done to predict hydrocarbon reactions with the graphite surfaces.[7]

Since the plasma will be dominated by hydrogen species, only reactions between impurity atoms or ions with the background plasma are considered. Reactions between two hydrocarbons are too unlikely. Therefore, four categories of reactions were investigated: electron impact ionization (including dissociative ionization), electron impact dissociation, proton impact ionization, and dissociative recombination.

Here we will show briefly how these cross sections or rate coefficients were approximated and present the results in a useful tabular form. A more thorough treatment of this plasma chemistry model, together with the surface reaction model, will be published elsewhere.[8] Two of the four reaction types were discussed[9] and plots of cross sections and reaction rates[10] were given in previous work.

After introducing the hydrocarbon reaction model, we look at an application of the model—an erosion/redeposition analysis of the Joint European Torus (JET)[23] MARK II carbon inner divertor. The improved hydrocarbon modeling capabilities in the WBC Monte Carlo impurity transport code allow us to explain an experimentally observed phenomenon in JET where much of the tritium used is trapped in layers of redeposited carbon in the plenum region near the inner divertor.

 © 2000 American Institute of Physics

Downloaded 21 Nov 2007 to 130.126.32.13. Redistribution subject to AIP license or copyright; see http://pop.aip.org/pop/copyright.jsp

TABLE I. Calculation of proton impact ionization rate coefficients from molar refraction.

	Molar refraction (cm^3/mol)			→	Molecular polarizability ($\times 10^{-24}$ cm^3)			→	Rate coefficient (cm^3/s)		
Formula	Calc. value	Lit. value[a]	Rel. error		Calc. value	Lit. value[b]	Rel. error		Calc. value	Lit. value[c]	Rel. error
CH	4.48				1.78				2.37		
CH_2	5.03				1.99				2.50		
CH_3	5.57				2.21				2.62		
CH_4	6.12	6.45	−5.13%		2.43	2.59	−6.44%		2.73	4.15	−34.2%
C_2H	8.42				3.34				3.14		
C_2H_2	8.97	8.58	4.52%		3.56	3.63	−2.07%		3.24	6.30	−48.6%
C_2H_3	9.51				3.77				3.33		
C_2H_4	10.06	10.34	−2.73%		3.99	4.25	−6.23%		3.42	5.00	−31.6%
C_2H_5	10.60			→	4.20			→	3.51		
C_2H_6	11.15	11.07	0.71%		4.42	4.45	−0.68%		3.59	3.90	−7.94%
C_3H	12.36				4.90				3.76		
C_3H_2	12.91				5.12				3.84		
C_3H_3	13.45				5.33				3.92		
C_3H_4	14.00	14.37	−2.58%		5.55	6.18	−10.22%		3.99		
C_3H_5	14.54				5.77				4.07		
C_3H_6	15.09	14.55	3.69%		5.98	5.96	0.35%		4.14		

[a]From Ref. 13.
[b]From Ref. 12.
[c]From Refs. 14 and 15.

TABLE II. Proton impact ionization rate coefficients.

Reactants	Products	Derived total rate (cm^3/s)	Experimental value (cm^3/s)	Reference
$H^+ + CH_4 \rightarrow$	0.5 $CH_4^+ + H$	3.8×10^{-9}	3.8×10^{-9}	14
	0.5 $CH_3^+ + H_2$		4.5×10^{-9}	
$H^+ + CH_3 \rightarrow$	0.5 $CH_3^+ + H$	3.6×10^{-9}	⋯	
	0.5 $CH_2^+ + H_2$		⋯	
$H^+ + CH_2 \rightarrow$	0.5 $CH_2^+ + H$	3.4×10^{-9}	⋯	
	0.5 $CH^+ + H_2$			
$H^+ + CH \rightarrow$	1.0 $CH^+ + H$	3.2×10^{-9}	⋯	
$H^+ + C_2H_6 \rightarrow$	0.33 $C_2H_5^+ + H_2$	5.0×10^{-9}	3.9×10^{-9}	14
	0.33 $C_2H_4^+ + H_2 + H$			16
	0.33 $C_2H_3^+ + H_2 + H_2$			
$H^+ + C_2H_5 \rightarrow$	0.33 $C_2H_5^+ + H$	4.9×10^{-9}	⋯	
	0.33 $C_2H_4^+ + H_2$			
	0.33 $C_2H_3^+ + H_2 + H$			
$H^+ + C_2^-H_4 \rightarrow$	0.33 $C_2H_4^+ + H$	4.8×10^{-9}	5.0×10^{-9}	17
	0.33 $C_2H_3^+ + H_2$			
	0.33 $C_2H_2^+ + H_2 + H$			
$H^+ + C_2H_3 \rightarrow$	0.33 $C_2H_3^+ + H$	4.6×10^{-9}	⋯	
	0.33 $C_2H_2^+ + H_2$			
	0.33 $C_2H^+ + H_2 + H$			
$H^+ + C_2H_2 \rightarrow$	0.5 $C_2H_2^+ + H$	4.5×10^{-9}	6.3×10^{-9}	17
	0.5 $C_2H^+ + H_2$			
$H^+ + C_2H \rightarrow$	1.00 $C_2H + H$	4.4×10^{-9}	⋯	
$H^+ + C_3H_6 \rightarrow$	0.33 $C_3H_6^+ + H$	5.8×10^{-9}	⋯	
	0.33 $C_3H_5^+ + H_2$			
	0.33 $C_3H_4^+ + H_2 + H$			
$H^+ + C_3H_5 \rightarrow$	0.33 $C_3H_5^+ + H$	5.7×10^{-9}	⋯	
	0.33 $C_3H_4^+ + H_2$			
	0.33 $C_3H_3^+ + H_2 + H$			
$H^+ + C_3H_4 \rightarrow$	0.33 $C_3H_4^+ + H$	5.9×10^{-9}	⋯	
	0.33 $C_3H_3^+ + H_2$			
	0.33 $C_3H_2^+ + H_2 + H$			
$H^+ + C_3H_3 \rightarrow$	0.33 $C_3H_3^+ + H$	5.5×10^{-9}	⋯	
	0.33 $C_3H_2^+ + H_2$			
	0.33 $C_3H^+ + H_2 + H$			
$H^+ + C_3H_2 \rightarrow$	0.5 $C_3H_2^+ + H$	5.4×10^{-9}	⋯	
	0.5 $C_3H^+ + H_2$			
$H^+ + C_3H \rightarrow$	1.0 $C_3H^+ + H$	5.2×10^{-9}	⋯	

II. PROTON IMPACT IONIZATION

Gioumousis and Stevenson compared experiments to the Langevin model[11] and found that the rate constant for anion–molecule collision process is related to the cross section, σ, by

$$k = \sigma v, \tag{1}$$

where v is the velocity of the ion. If a reaction is assumed to take place at every collision the cross section is given by

$$\sigma = \frac{2\pi}{v}\left(\frac{e^2\alpha}{M_r}\right)^{1/2}, \tag{2}$$

where e is the ion charge, α is the molecular polarizability of the reactant molecule, and M_r is the reduced mass of the reacting system. By substituting this expression for the cross section into (1), we get a useful formula for calculating reaction rates for ion–molecule reactions,

$$k = 2\pi\left(\frac{e^2\alpha}{M_r}\right)^{1/2}. \tag{3}$$

Unfortunately, molecular polarizability data are not often available. To make matters worse, the relationship between polarizability and reaction rates means that most molecules with unknown reaction rates also have unknown polarizabilities. However, the unknown molecular polarizabilities can be calculated from the molecules' molar refractions according to the Lorentz–Lorenz relation

$$\alpha = \frac{3}{4\pi N_A}R, \tag{4}$$

where N_A is Avogadro's number, and R is the molar refraction. For many compounds, the molar refraction is additive for the bonds present in the molecule.[12] For our purposes, R is approximately proportional to the number of each type of atom present. A least-squares fit was done using the six

Downloaded 21 Nov 2007 to 130.126.32.13. Redistribution subject to AIP license or copyright; see http://pop.aip.org/pop/copyright.jsp

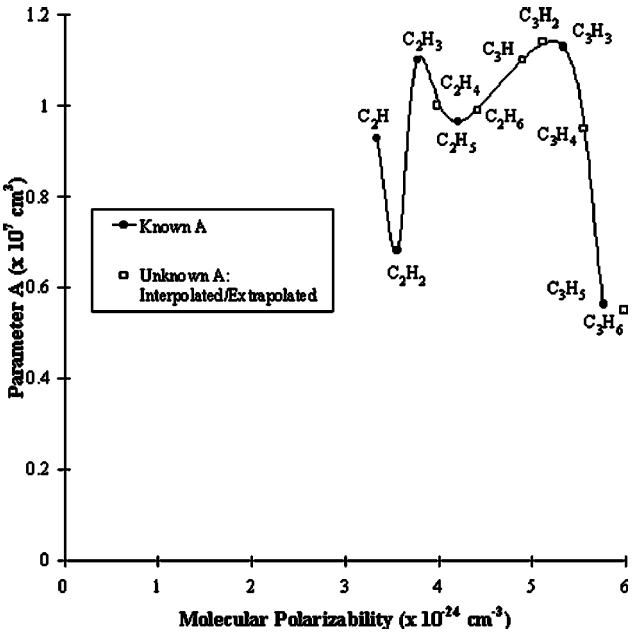

FIG. 1. Parameter A vs polarizability.

TABLE IV. Known parameters for electron impact ionization.

Molecule	E_{th} (eV)	E_{max} (eV)	σ_{max} (cm^2)	λ (eV)
CH	10.64	70	2.03×10^{-16}	470.6
CH_2	10.40	80	2.38×10^{-16}	958.7
CH_3	9.84	79	2.73×10^{-16}	582.7
CH_4	12.51	83	3.89×10^{-16}	757.9
C_2H_2	11.40	87	5.07×10^{-16}	633.6
C_2H_4	10.51	90	5.86×10^{-16}	667.8
C_2H_6	11.52	86	6.27×10^{-16}	742.2

known molar refraction values for CH_4, C_2H_6, C_2H_4, C_2H_2, C_3H_6, and C_3H_4 listed in Table I, and the resulting relationship is

$$R = 3.939(\text{No. of C atoms}) + 0.5452(\text{No. of H atoms}). \quad (5)$$

Comparing this method to the literature values shows up to about 5% error in predicting the molar refractions. These values can therefore be used in (4) to calculate polarizabilities, which can in turn be used in (3) to calculate the total proton impact ionization rate coefficient for every hydrocarbon molecule of interest (see Table II). Equation (4) may not include some low-frequency contributions to the static polar-

TABLE III. Dissociative recombination rate coefficients.

Reactants	Products	Derived total rate (cm^3/s)	Experimental value (cm^3/s)	Reference
$e^-+CH_4^+$	0.25 CH_3+H	$5.4\times10^{-8}T^{-0.84}<1$ eV	3.8×10^{-9} at 0.0257 eV	2
	0.75 CH_2+H_2	$5.4\times10^{-8}T^{-1.05}>1$ eV	4.5×10^{-9} at 0.0259 eV	
$e^-+CH_3^+$	1.00 CH_2+H	$6.8\times10^{-8}T^{-0.770}<1$ eV	⋯	2
		$6.8\times10^{-8}T^{-0.979}>1$ eV		
$e^-+CH_2^+$	1.00 $CH+H$	$1.0\times10^{-7}T^{-0.544}<1$ eV	⋯	2
		$1.0\times10^{-7}T^{-1.21}>1$ eV		
e^-+CH^+	1.00 $C+H$	$7.0\times10^{-8}T^{-0.553}<1$ eV	⋯	2
		$7.0\times10^{-8}T^{-1.18}>1$ eV		
$e^-+C_2H_6^+$	0.50 C_2+H_5+H	$9.9\times10^{-8}T^{-0.50}$	⋯	17
	0.50 $C_2H_4+H_2$			
$e^-+C_2H_5^+$	0.50 C_2+H_4+H	$9.65\times10^{-8}T^{-0.50}$	6.0×10^{-7} at 0.0259 eV	4
	0.50 $C_2H_3+H_2$			
$e^-+C_2H_4^+$	0.50 C_2+H_3+H	$1.00\times10^{-7}T^{-0.50}$	⋯	
	0.50 $C_2H_2+H_2$			
$e^-+C_2H_3^+$	0.50 C_2+H_2+H	$1.10\times10^{-7}T^{-0.50}$	1.6×10^{-6} at 0.008 63 eV	18
	0.50 C_2H+H_2		4.5×10^{-7} at 0.0259 eV	4
$e^-+C_2H_2^+$	0.33 C_2+H+H	$6.81\times10^{-8}T^{-0.50}$	1×10^{-6} at 0.008 63 eV	18
	0.33 $CH+CH$		2.7×10^{-7} at 0.0259 eV	4
	0.33 $2C+2H$			
$e^-+C_2H^+$	0.50 $2C+H$	$9.28\times10^{-8}T^{-0.50}$	1×10^{-6} at 0.008 63 eV	18
	0.50 $CH+C$			
$e^-+C_3H_6^+$	0.50 C_3H_5+H	$5.50\times10^{-8}T^{-0.50}$	⋯	
	0.50 $C_3H_4+H_2$			
$e^-+C_3H_5^+$	0.50 C_3H_4+H	$5.63\times10^{-8}T^{-0.50}$	3.5×10^{-7} at 0.0259 eV	4
	0.50 $C_3H_3+H_2$			
$e^-+C_3H_4^+$	0.50 C_3H_3+H	$1.10\times10^{-7}T^{-0.50}$	⋯	
	0.50 $C_3H_2+H_2$			
$e^-+C_3H_3^+$	0.50 C_3H_2+H	$1.10\times10^{-7}T^{-0.50}$	7.0×10^{-7} at 0.0259 eV	3
	0.50 C_3H+H_2		7.0×10^{-7} at 0.0259 eV	4
$e^-+C_3H_2^+$	0.50 C_2H+CH	$1.10\times10^{-7}T^{-0.50}$	⋯	
	0.50 C_3H+H			
$e^-+C_3H^+$	0.33 $CH+2C$	$1.10\times10^{-7}T^{-0.50}$	⋯	
	0.33 C_2H+C			
	0.33 $3C+H$			

Downloaded 21 Nov 2007 to 130.126.32.13. Redistribution subject to AIP license or copyright; see http://pop.aip.org/pop/copyright.jsp

TABLE V. Electron impact ionization cross sections.

Reaction	Cross section (cm^2)[a]	Energy range (eV)	Reference
$e^- + CH_4 \rightarrow CH_4^+ + 2e^-$	$1.8\times10^{-16}\left[1-\left(\frac{90-E}{90-12.6}\right)^2\right]$	$12.6<E<90$	2
			19
	$1.8\times10^{-16}\exp\left[\frac{90-E}{748}\right]$	$E>90$	
$\rightarrow CH_3^+ + H + 2e^-$	$1.4\times10^{-16}\left[1-\left(\frac{100-E}{100-14.3}\right)^2\right]$	$14.3<E<100$	
	$1.4\times10^{-16}\exp\left[\frac{100-E}{799}\right]$	$E>100$	
$e^- + CH_3 \rightarrow CH_3^+ + 2e^-$	$1.8\times10^{-16}\left[1-\left(\frac{95-E}{95-12.6}\right)^2\right]$	$12.6<E<95$	2
	$1.8\times10^{-16}\exp\left[\frac{95-E}{767}\right]$	$E>95$	
$\rightarrow CH_2^+ + H + 2e^-$	$1.0\times10^{-16}\left[1-\left(\frac{85-E}{85-15}\right)^2\right]$	$15<E<85$	
	$1.0\times10^{-16}\exp\left[\frac{85-E}{832}\right]$	$E>85$	
$e^- + CH_2 \rightarrow CH_2^+ + 2e^-$	$1.8\times10^{-16}\left[1-\left(\frac{95-E}{95-12.6}\right)^2\right]$	$12.6<E<95$	2
	$1.8\times10^{-16}\exp\left[\frac{95-E}{767}\right]$	$E>95$	
$\rightarrow CH^+ + H + 2e^-$	$6.5\times10^{-17}\left[1-\left(\frac{95-E}{95-17.9}\right)^2\right]$	$17.9<E<95$	
	$6.5\times10^{-17}\exp\left[\frac{95-E}{800}\right]$	$E>95$	
$e^- + CH \rightarrow CH^+ + 2e^-$	$1.8\times10^{-16}\left[1-\left(\frac{95-E}{95-12.6}\right)^2\right]$	$12.6<E<95$	2
	$1.8\times10^{-16}\exp\left[\frac{95-E}{746}\right]$	$E>95$	
$\rightarrow C^+ + H + 2e^-$	$3.1\times10^{-17}\left[1-\left(\frac{95-E}{95-17}\right)^2\right]$	$17<E<95$	
	$3.1\times10^{-17}\exp\left[\frac{95-E}{816}\right]$	$E>95$	
$e^- + C_2H_6 \rightarrow C_2H_6^+ + 2e^-$	$1.32\times10^{-16}\left[1-\left(\frac{86-E}{86-10}\right)^2\right]$	$10<E<86$	19
			5
	$1.32\times10^{-16}\exp\left[\frac{86-E}{742}\right]$	$E>86$	
$\rightarrow C_2H_5^+ + H + 2e^-$	$8.66\times10^{-17}\left[1-\left(\frac{86-E}{86-12}\right)^2\right]$	$12<E<86$	
	$8.66\times10^{-17}\exp\left[\frac{86-E}{742}\right]$	$E>86$	
$\rightarrow C_2H_4^+ + H_2 + 2e^-$	$4.37\times10^{-16}\left[1-\left(\frac{86-E}{86-12}\right)^2\right]$	$12<E<86$	
	$4.37\times10^{-16}\exp\left[\frac{86-E}{742}\right]$	$E>86$	
$e^- + C_2H_5 \rightarrow C_2H_5^+ + 2e^-$	$1.24\times10^{-16}\left[1-\left(\frac{89-E}{89-10}\right)^2\right]$	$10<E<89$	
	$1.24\times10^{-16}\exp\left[\frac{89-E}{717}\right]$	$E>89$	
$\rightarrow C_2H_4^+ + H + 2e^-$	$8.11\times10^{-17}\left[1-\left(\frac{89-E}{89-12}\right)^2\right]$	$12<E<89$	
	$8.11\times10^{-17}\exp\left[\frac{89-E}{717}\right]$	$E>89$	
$\rightarrow C_2H_3^+ + H + 2e^-$	$4.10\times10^{-16}\left[1-\left(\frac{89-E}{89-12}\right)^2\right]$	$12<E<89$	
	$4.10\times10^{-16}\exp\left[\frac{89-E}{717}\right]$	$E>89$	
$e^- + C_2H_4 \rightarrow C_2H_4^+ + 2e^-$	$1.15\times10^{-16}\left[1-\left(\frac{90-E}{90-10}\right)^2\right]$	$10<E<90$	5

Downloaded 21 Nov 2007 to 130.126.32.13. Redistribution subject to AIP license or copyright; see http://pop.aip.org/pop/copyright.jsp

TABLE V. (*Continued*.)

Reaction	Cross section (cm^2)[a]	Energy range (eV)	Reference
	$1.15\times10^{-16}\exp\left[\frac{90-E}{668}\right]$	$E>90$	
$\rightarrow C_2H_3^+ + H + 2e^-$	$7.57\times10^{-17}\left[1-\left(\frac{90-E}{90-12}\right)^2\right]$	$12<E<90$	
	$7.57\times10^{-17}\exp\left[\frac{90-E}{668}\right]$	$E>90$	
$\rightarrow C_2H_2^+ + H_2 + 2e^-$	$3.82\times10^{-16}\left[1-\left(\frac{90-E}{90-12}\right)^2\right]$	$12<E<90$	
	$3.82\times10^{-16}\exp\left[\frac{90-E}{668}\right]$	$E>90$	
$e^- + C_2H_3 \rightarrow C_2H_3^+ + 2e^-$	$1.07\times10^{-16}\left[1-\left(\frac{86-E}{86-10}\right)^2\right]$	$10<E<86$	
	$1.07\times10^{-16}\exp\left[\frac{86-E}{646}\right]$	$E>86$	
$\rightarrow C_2H_2^+ + H + 2e^-$	$7.02\times10^{-17}\left[1-\left(\frac{86-E}{86-12}\right)^2\right]$	$12<E<86$	
	$7.02\times10^{-17}\exp\left[\frac{86-E}{646}\right]$	$E>86$	
$\rightarrow C_2H^+ + H_2 + 2e^-$	$3.55\times10^{-16}\left[1-\left(\frac{86-E}{86-12}\right)^2\right]$	$12<E<86$	
	$3.55\times10^{-16}\exp\left[\frac{86-E}{646}\right]$	$E>86$	
$e^- + C_2H_2 \rightarrow C_2H_2^+ + 2e^-$	$2.96\times10^{-16}\left[1-\left(\frac{87-E}{87-10}\right)^2\right]$	$12<E<87$	5
	$2.96\times10^{-16}\exp\left[\frac{87-E}{634}\right]$	$E>87$	
$\rightarrow C_2H^+ + H + 2e^-$	$1.94\times10^{-16}\left[1-\left(\frac{87-E}{87-12}\right)^2\right]$	$12<E<87$	
	$1.94\times10^{-16}\exp\left[\frac{87-E}{634}\right]$	$E>87$	
$e^- + C_2H \rightarrow C_2H^+ + 2e^-$	$2.71\times10^{-16}\left[1-\left(\frac{84-E}{84-10}\right)^2\right]$	$12<E<84$	
	$2.71\times10^{-16}\exp\left[\frac{84-E}{575}\right]$	$E>84$	
$\rightarrow C^+ + C + H + 2e^-$	$1.94\times10^{-16}\left[1-\left(\frac{84-E}{84-12}\right)^2\right]$	$12<E<84$	
	$1.94\times10^{-16}\exp\left[\frac{84-E}{575}\right]$	$E>84$	
$e^- + C_3H_6 \rightarrow C_3H_6^+ + 2e^-$	$1.79\times10^{-16}\left[1-\left(\frac{98-E}{98-10}\right)^2\right]$	$12<E<98$	
	$1.79\times10^{-16}\exp\left[\frac{98-E}{688}\right]$	$E>98$	
$\rightarrow C_3H_5^+ + H + 2e^-$	$1.18\times10^{-16}\left[1-\left(\frac{98-E}{98-12}\right)^2\right]$	$10<E<98$	
	$1.18\times10^{-16}\exp\left[\frac{98-E}{688}\right]$	$E>98$	
$\rightarrow C_3H_4^+ + 2H + 2e^-$	$5.95\times10^{-16}\left[1-\left(\frac{98-E}{98-12}\right)^2\right]$	$12<E<98$	
	$5.95\times10^{-16}\exp\left[\frac{98-E}{688}\right]$	$E>98$	
$e^- + C_3H_5 \rightarrow C_3H_5^+ + 2e^-$	$1.71\times10^{-16}\left[1-\left(\frac{97-E}{97-10}\right)^2\right]$	$12<E<97$	
	$1.71\times10^{-16}\exp\left[\frac{97-E}{652}\right]$	$E>97$	
$\rightarrow C_3H_4^+ + H + 2e^-$	$1.21\times10^{-16}\left[1-\left(\frac{97-E}{97-12}\right)^2\right]$	$10<E<97$	
	$1.21\times10^{-16}\exp\left[\frac{97-E}{652}\right]$	$E>97$	

Downloaded 21 Nov 2007 to 130.126.32.13. Redistribution subject to AIP license or copyright; see http://pop.aip.org/pop/copyright.jsp

TABLE V. (*Continued*.)

Reaction	Cross section (cm^2)[a]	Energy range (eV)	Reference
$\rightarrow C_3H_3^+ + 2H + 2e^-$	$5.67\times10^{-16}\left[1-\left(\frac{97-E}{97-12}\right)^2\right]$	$12<E<97$	
	$5.67\times10^{-16}\exp\left[\frac{97-E}{652}\right]$	$E>97$	
$e^- + C_3H_4 \rightarrow C_3H_4^+ + 2e^-$	$1.63\times10^{-16}\left[1-\left(\frac{95-E}{95-10}\right)^2\right]$	$12<E<95$	
	$1.63\times10^{-16}\exp\left[\frac{95-E}{617}\right]$	$E>95$	
$\rightarrow C_3H_3^+ + H + 2e^-$	$1.07\times10^{-16}\left[1-\left(\frac{95-E}{95-12}\right)^2\right]$	$12<E<95$	
	$1.07\times10^{-16}\exp\left[\frac{95-E}{617}\right]$	$E>95$	
$\rightarrow C_3H_2^+ + 2H + 2e^-$	$5.40\times10^{-16}\left[1-\left(\frac{95-E}{95-12}\right)^2\right]$	$12<E<95$	
	$5.40\times10^{-16}\exp\left[\frac{95-E}{617}\right]$	$E>95$	
$e^- + C_3H_3 \rightarrow C_3H_3^+ + 2e^-$	$1.54\times10^{-16}\left[1-\left(\frac{94-E}{94-10}\right)^2\right]$	$10<E<94$	
	$1.54\times10^{-16}\exp\left[\frac{94-E}{581}\right]$	$E>94$	
$\rightarrow C_3H_2^+ + H + 2e^-$	$1.01\times10^{-16}\left[1-\left(\frac{94-E}{94-12}\right)^2\right]$	$12<E<94$	
	$1.01\times10^{-16}\exp\left[\frac{94-E}{581}\right]$	$E>94$	
$\rightarrow C_3H^+ + 2H + 2e^-$	$5.12\times10^{-16}\left[1-\left(\frac{94-E}{94-12}\right)^2\right]$	$12<E<94$	
	$5.12\times10^{-16}\exp\left[\frac{94-E}{581}\right]$	$E>94$	
$e^- + C_3H_2 \rightarrow C_3H_2^+ + 2e^-$	$4.39\times10^{-16}\left[1-\left(\frac{93-E}{93-10}\right)^2\right]$	$10<E<93$	
	$4.39\times10^{-16}\exp\left[\frac{93-E}{546}\right]$	$E>93$	
$\rightarrow C_3H^+ + H + 2e^-$	$2.88\times10^{-16}\left[1-\left(\frac{93-E}{93-12}\right)^2\right]$	$12<E<93$	
	$2.88\times10^{-16}\exp\left[\frac{93-E}{546}\right]$	$E>93$	
$e^- + C_3H \rightarrow C_3H^+ + 2e^-$	$6.85\times10^{-16}\left[1-\left(\frac{91-E}{91-10}\right)^2\right]$	$10<E<91$	
	$6.85\times10^{-16}\exp\left[\frac{91-E}{511}\right]$	$E>91$	

[a]All cross sections are zero below the threshold energy.

izability and may therefore be low by up to 30%.[12] In fact, by comparing the estimates to the six known polarizabilities and rate coefficients, we see up to 10% and 50% error, respectively, as shown in Table I. While the rate coefficients quoted are for thermal energies (300 K), at low energies (from thermal up to the few electron volt region we are interested in) there is little energy dependence in the rate coefficients. So these numbers are good enough for our purposes.

The branching ratios, however, do not remain constant up to a few electron volts. At thermal energies where the experimental measurements were taken, one channel tends to dominate over the others. However, some temperature-

TABLE VI. Known parameters for electron impact dissociation.

Molecule	E_{th} (eV)	E_{max} (eV)	σ_{max} (cm^2)	λ (eV)
$e^- + C_xH_y \rightarrow C_xH_{y-1} + H + e^-$				
CH	10	25	6.0×10^{-17}	77
CH_2	10	25	7.33×10^{-17}	77
CH_3	10	25	1.27×10^{-16}	77
CH_4	10	25	1.4×10^{-16}	77
$e^- + C_xH_y \rightarrow C_xH_{y-2} + H_2 + e^-$				
CH	10	18	⋯	11.4
CH_2	10	18	3.67×10^{-17}	11.4
CH_3	10	18	6.33×10^{-17}	11.4
CH_4	10	18	7.3×10^{-17}	11.4

Downloaded 21 Nov 2007 to 130.126.32.13. Redistribution subject to AIP license or copyright; see http://pop.aip.org/pop/copyright.jsp

TABLE VII. Electron impact dissociation cross sections.

Reaction		Cross section (cm^2)[a]	Energy range (eV)	Reference
$e^- + CH_4$	$\rightarrow CH_3 + H + e^-$	$1.4\times10^{-16}\left[1-\left(\frac{25-E}{25-10}\right)^2\right]$	$10<E<25$	2
				6
		$1.4\times10^{-16}\exp\left[\frac{25-E}{77}\right]$	$E>25$	
	$\rightarrow CH_2 + 2H + e^-$	$7.3\times10^{-17}\left[1-\left(\frac{18-E}{18-10}\right)^2\right]$	$10<E<18$	
		$7.3\times10^{-17}\exp\left[\frac{18-E}{11.4}\right]$	$E>18$	
$e^- + CH_3$	$\rightarrow CH_2 + H + e^-$	$1.27\times10^{-16}\left[1-\left(\frac{25-E}{25-10}\right)^2\right]$	$10<E<25$	2
		$1.27\times10^{-16}\exp\left[\frac{25-E}{77}\right]$	$E>25$	
	$\rightarrow CH + 2H + e^-$	$6.33\times10^{-17}\left[1-\left(\frac{18-E}{18-10}\right)^2\right]$	$10<E<18$	
		$6.33\times10^{-17}\exp\left[\frac{18-E}{11.4}\right]$	$E>18$	
$e^- + CH_2$	$\rightarrow CH + H + e^-$	$7.33\times10^{-17}\left[1-\left(\frac{25-E}{25-10}\right)^2\right]$	$10<E<25$	2
		$7.33\times10^{-17}\exp\left[\frac{25-E}{77}\right]$	$E>25$	
	$\rightarrow C + 2H + e^-$	$3.67\times10^{-17}\left[1-\left(\frac{18-E}{18-10}\right)^2\right]$	$10<E<18$	
		$3.67\times10^{-17}\exp\left[\frac{18-E}{11.4}\right]$	$E>18$	
$e^- + CH$	$\rightarrow C + H + e^-$	$6.0\times10^{-17}\left[1-\left(\frac{25-E}{25-10}\right)^2\right]$	$10<E<25$	2
		$6.0\times10^{-17}\exp\left[\frac{25-E}{77}\right]$	$E>25$	
$e^- + C_2H_6$	$\rightarrow C_2 + H_5 + H + e^-$	$3.34\times10^{-16}\left[1-\left(\frac{25-E}{25-10}\right)^2\right]$	$10<E<25$	
		$3.34\times10^{-16}\exp\left[\frac{25-E}{77}\right]$	$E>25$	
	$\rightarrow C_2 + H_4 + 2H + e^-$	$1.67\times10^{-16}\left[1-\left(\frac{18-E}{18-10}\right)^2\right]$	$10<E<18$	
		$1.67\times10^{-16}\exp\left[\frac{18-E}{11.4}\right]$	$E>18$	
$e^- + C_2H_5$	$\rightarrow C_2 + H_4 + H + e^-$	$3.28\times10^{-16}\left[1-\left(\frac{25-E}{25-10}\right)^2\right]$	$10<E<25$	
		$3.28\times10^{-16}\exp\left[\frac{25-E}{77}\right]$	$E>25$	
	$\rightarrow C_2 + H_3 + 2H + e^-$	$1.64\times10^{-16}\left[1-\left(\frac{18-E}{18-10}\right)^2\right]$	$10<E<18$	
		$1.64\times10^{-16}\exp\left[\frac{18-E}{11.4}\right]$	$E>18$	
$e^- + C_2H_4$	$\rightarrow C_2 + H_3 + H + e^-$	$3.13\times10^{-16}\left[1-\left(\frac{25-E}{25-10}\right)^2\right]$	$10<E<25$	
		$3.13\times10^{-16}\exp\left[\frac{25-E}{77}\right]$	$E>25$	
	$\rightarrow C_2 + H_2 + 2H + e^-$	$1.56\times10^{-16}\left[1-\left(\frac{18-E}{18-10}\right)^2\right]$	$10<E<18$	
		$1.56\times10^{-16}\exp\left[\frac{18-E}{11.4}\right]$	$E>18$	

Downloaded 21 Nov 2007 to 130.126.32.13. Redistribution subject to AIP license or copyright; see http://pop.aip.org/pop/copyright.jsp

TABLE VII. (*Continued*.)

Reaction		Cross section (cm^2)[a]	Energy range (eV)	Reference
$e^- + C_2H_3$	$\rightarrow C_2 + H_2 + H + e^-$	$2.84\times10^{-16}\left[1-\left(\frac{25-E}{25-10}\right)^2\right]$	$10<E<25$	
		$2.84\times10^{-16}\exp\left[\frac{25-E}{77}\right]$	$E>25$	
	$\rightarrow C_2 + H + 2H + e^-$	$1.42\times10^{-16}\left[1-\left(\frac{18-E}{18-10}\right)^2\right]$	$10<E<18$	
		$1.42\times10^{-16}\exp\left[\frac{18-E}{11.4}\right]$	$E>18$	
$e^- + C_2H_2$	$\rightarrow C_2 + H + H + e^-$	$4.06\times10^{-16}\left[1-\left(\frac{25-E}{25-10}\right)^2\right]$	$10<E<25$	
		$4.06\times10^{-16}\exp\left[\frac{25-E}{77}\right]$	$E>25$	
$e^- + C_2H$	$\rightarrow C + Cs + H + e^-$	$3.60\times10^{-16}\left[1-\left(\frac{25-E}{25-10}\right)^2\right]$	$10<E<25$	
		$3.60\times10^{-16}\exp\left[\frac{25-E}{77}\right]$	$E>25$	
$e^- + C_3H_6$	$\rightarrow C_3H_5 + H + e^-$	$4.67\times10^{-16}\left[1-\left(\frac{25-E}{25-10}\right)^2\right]$	$10<E<25$	
		$4.76\times10^{-16}\exp\left[\frac{25-E}{77}\right]$	$E>25$	
	$\rightarrow C_3 + H_4 + 2H + e^-$	$2.38\times10^{-16}\left[1-\left(\frac{18-E}{18-10}\right)^2\right]$	$10<E<18$	
		$2.38\times10^{-16}\exp\left[\frac{18-E}{11.4}\right]$	$E>18$	
$e^- + C_3H_5$	$\rightarrow C_3H_4 + H + e^-$	$4.53\times10^{-16}\left[1-\left(\frac{25-E}{25-10}\right)^2\right]$	$10<E<25$	
		$4.53\times10^{-16}\exp\left[\frac{25-E}{77}\right]$	$E>77$	
	$\rightarrow C_3 + H_3 + 2H + e^-$	$2.27\times10^{-16}\left[1-\left(\frac{18-E}{18-10}\right)^2\right]$	$10<E<18$	
		$2.27\times10^{-16}\exp\left[\frac{18-E}{11.4}\right]$	$E>18$	
$e^- + C_3H_4$	$\rightarrow C_3H_3 + H + e^-$	$4.31\times10^{-16}\left[1-\left(\frac{25-E}{25-10}\right)^2\right]$	$10<E<25$	
		$4.31\times10^{-16}\exp\left[\frac{25-E}{77}\right]$	$E>25$	
	$\rightarrow C_3 + H_2 + 2H + e^-$	$2.16\times10^{-16}\left[1-\left(\frac{18-E}{18-10}\right)^2\right]$	$10<E<18$	
		$2.16\times10^{-16}\exp\left[\frac{18-E}{11.4}\right]$	$E>18$	
$e^- + C_3H_3$	$\rightarrow C_3H_2 + H + e^-$	$4.10\times10^{-16}\left[1-\left(\frac{25-E}{25-10}\right)^2\right]$	$10<E<25$	
		$4.10\times10^{-16}\exp\left[\frac{25-E}{77}\right]$	$E>25$	
	$\rightarrow C_3H + 2H + e^-$	$2.05\times10^{-16}\left[1-\left(\frac{18-E}{18-10}\right)^2\right]$	$10<E<18$	
		$2.05\times10^{-16}\exp\left[\frac{18-E}{11.4}\right]$	$E>18$	
$e^- + C_3H_2$	$\rightarrow C_3H + H + e^-$	$5.82\times10^{-16}\left[1-\left(\frac{25-E}{25-10}\right)^2\right]$	$10<E<25$	
		$5.82\times10^{-16}\exp\left[\frac{25-E}{77}\right]$	$E>25$	
$e^- + C_3H$	$\rightarrow 3C + H + e^-$	$5.48\times10^{-16}\left[1-\left(\frac{25-E}{25-10}\right)^2\right]$	$10<E<25$	
		$5.48\times10^{-16}\exp\left[\frac{25-E}{77}\right]$	$E>25$	

[a]All cross sections are zero below the threshold energy.

Downloaded 21 Nov 2007 to 130.126.32.13. Redistribution subject to AIP license or copyright; see http://pop.aip.org/pop/copyright.jsp

TABLE VIII. Summary of WBC code analysis of carbon chemical sputtering of the JET Mark II inner divertor.

Plasma temperature (eV)	Overall carbon redeposition fraction	Fraction of redeposited particles that are neutral/ionized	Fraction of chem. sputtered carbon going to inner louver region
1	0.86	0.79/0.21	0.095
3	0.93	0.57/0.43	0.051
10	0.95	0.17/0.83	0.006

dependent results indicate that the product distribution becomes more evenly distributed as temperature increases, reaching a 50–50 distribution at ~ 0.2 eV.[15] At the temperatures that we are interested in ($\sim 1-3$eV), we have assumed that all reactions produce an even distribution of possible products.

III. DISSOCIATIVE RECOMBINATION

The reaction rate for dissociative recombination is known to be inversely proportional to temperature. The mathematical approximation used for these reactions is

$$\langle \sigma v \rangle = \frac{A}{T^B}, \tag{6}$$

where A and B are parameters to be determined. The reaction rates as functions of temperature have only been published for the methane family.[2] In these lighter hydrocarbons, there is a noticeable bend in the $\langle \sigma v \rangle$ vs T plot, so the reaction rate has been split up into two sections, each with their own A and B, covering the temperature ranges $T<1$ and $T>1$ eV. For the heavier ions, the rate can be approximated by just one function for all energies. Of the twelve heavier hydrocarbons of importance, there are experimentally determined values of the reaction rate at one energy (usually 300 K) in the literature for six of them. The energy dependence was known[17] for several of these ions to be $\langle \sigma v \rangle \propto T^{-1/2}$, i.e., $B=1/2$. Using this energy dependence, together with the one data point, allows us to solve for the remaining parameter, A, for six of the ions.

The remaining six hydrocarbons present more of a challenge. Bates had proposed that the dissociative recombination rate is proportional to the number of bonds that can be broken. There is some disagreement about whether or not this is true, especially for more complex ions,[3] and since the reaction rates that we know so far do not seem to follow this type of a trend, another method of estimation must be employed. If we assume that the rate of dissociative recombination again depends on the polarizability of the ion and we use the same value of $B=1/2$, then it becomes rather easy to find these remaining reaction rates. A graph was constructed of the known values of the parameter A versus the molecular polarizability of the corresponding molecule. This is shown in Fig. 1. The value of A is found for five of the six remaining hydrocarbons by interpolating from this graph and by extrapolation for the other.

The branching ratios for the methane family have previously been published.[2] The data available on branching ratios

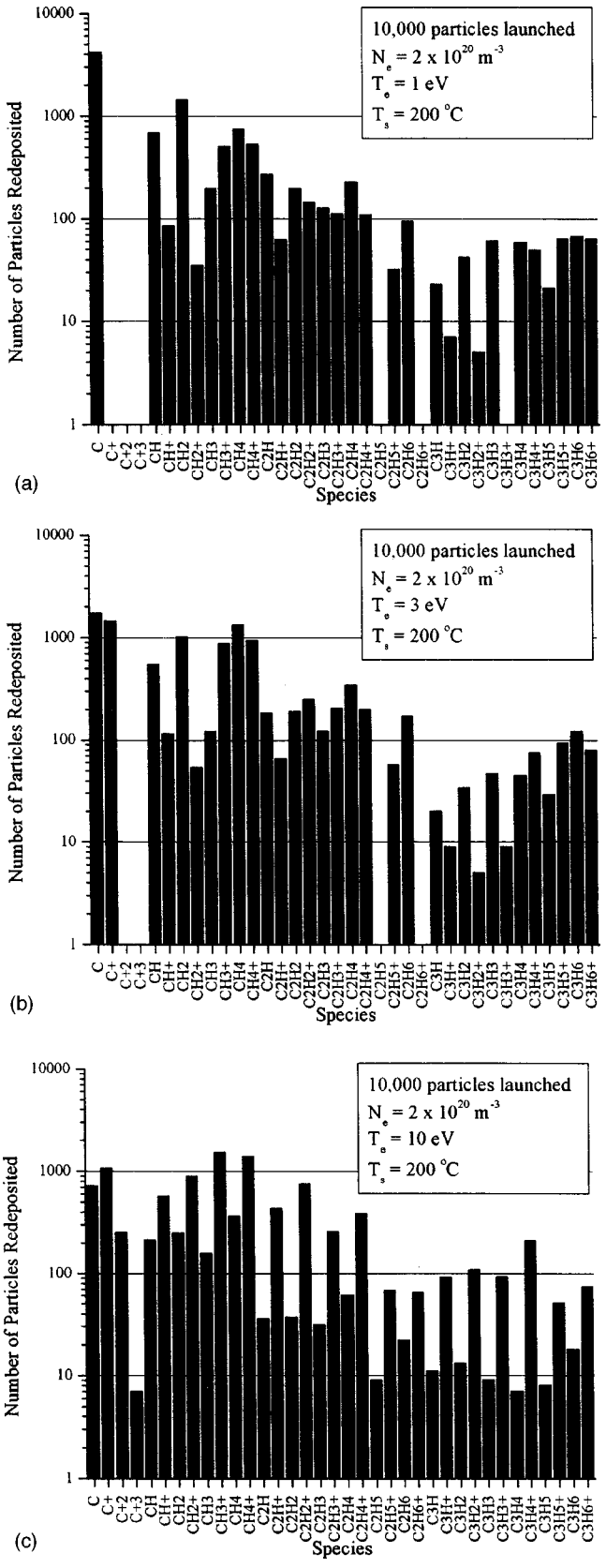

FIG. 2. (a) Carbon/hydrocarbon redeposited species from WBC analysis of the JET Mark II inner divertor with 1 eV plasma temperature. (b) Carbon/hydrocarbon redeposited species from WBC analysis of the JET Mark II inner divertor with 3 eV plasma temperature. (c) Carbon/hydrocarbon redeposited species from WBC analysis of the JET Mark II inner divertor with 10 eV plasma temperature.

Downloaded 21 Nov 2007 to 130.126.32.13. Redistribution subject to AIP license or copyright; see http://pop.aip.org/pop/copyright.jsp

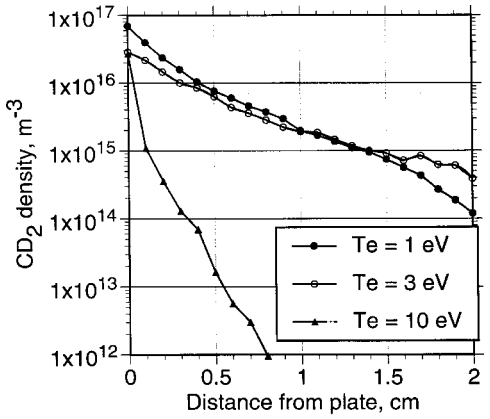

FIG. 3. Average CD_2 molecular density as a function of perpendicular distance from divertor plate. From WBC Monte Carlo code simulation of carbon chemical sputtering of JET MK-2 inner divertor, tile 4. For constant near-surface plasma density of $N_e = 2\times10^{20}$ $m^{-2}\,s^{-1}$ assumed for comparison purposes.

for some of the heavier hydrocarbons indicate that the product distributions are split evenly among the possible channels.[17] In our model, we use an even branching ratio for the dissociative recombination of these heavier molecules. The reaction rates are summarized in Table III. Note that the rate coefficients are in cubic centimeters per second and temperatures are in electron volts.

IV. ELECTRON IMPACT IONIZATION

The cross sections for electron impact ionization are approximated by a quadratic function in the region between the threshold energy, E_{th}, and the energy at which the maximum cross section occurs, E_{max}. At energies above E_{max}, the cross sections decay exponentially. They are therefore fit to four parameters: E_{th}, E_{max}, σ_{max}, and λ, according to

$$\sigma(E) = 0 \quad (E < E_{th}), \tag{7a}$$

$$\sigma(E) = \sigma_{max}\left[1 - \frac{(E_{max}-E)^2}{(E_{max}-E_{th})^2}\right] \quad (E_{th} < E < E_{max}), \tag{7b}$$

$$\sigma(E) = \sigma_{max}\exp\left[\frac{-(E-E_{max})}{\lambda}\right] \quad (E > E_{max}). \tag{7c}$$

Energy-dependent cross sections for CH, CH_2, CH_3, CH_4, C_2H_2, C_2H_4, and C_2H_6 were found in the literature.[2,5,19] The plots of σ vs E were fit to the above-mentioned functional form, yielding the parameters shown in Table IV.

Fortunately, ionization potentials are known for most of the remaining molecules[12] and are consistently around 10 eV. The remaining three parameters must be fit to the known graphs. If we again assume that the ionization cross section has some dependence on the polarizability of the molecule, as we did with the proton impact ionization reactions, then we can obtain estimates for the remaining three parameters based on the number of carbon and hydrogen atoms in each molecule. With those known, we have a good guess at the electron impact ionization cross section at any energy.

The energy at which the maximum cross section occurs, E_{max}, does not seem to vary much for the seven known values such that any value between 70 and 90 would be reasonable. However there are some assumptions we can make from the data. It seems that from the methane family data E_{max} tends to increase as the number of hydrogen atoms, H, increases. E_{max} also seems to increase as we move from the CH_y to the C_2H_y family, i.e., with increasing C. The approximate relationship used is

$$E_{max} = (7.71\,\text{eV})\text{C} + (1.31\,\text{eV})\text{H} + 67.0\,\text{eV}. \tag{8}$$

The maximum cross section, σ_{max}, shows a more definite dependence on C and H. There is an obvious increase with both the number of carbon and hydrogen atoms. The relationship used for the fit is

$$\sigma_{max} = (2.36\text{C} + 0.413\text{H} - 0.631)\times10^{-16}\,\text{cm}^2. \tag{9}$$

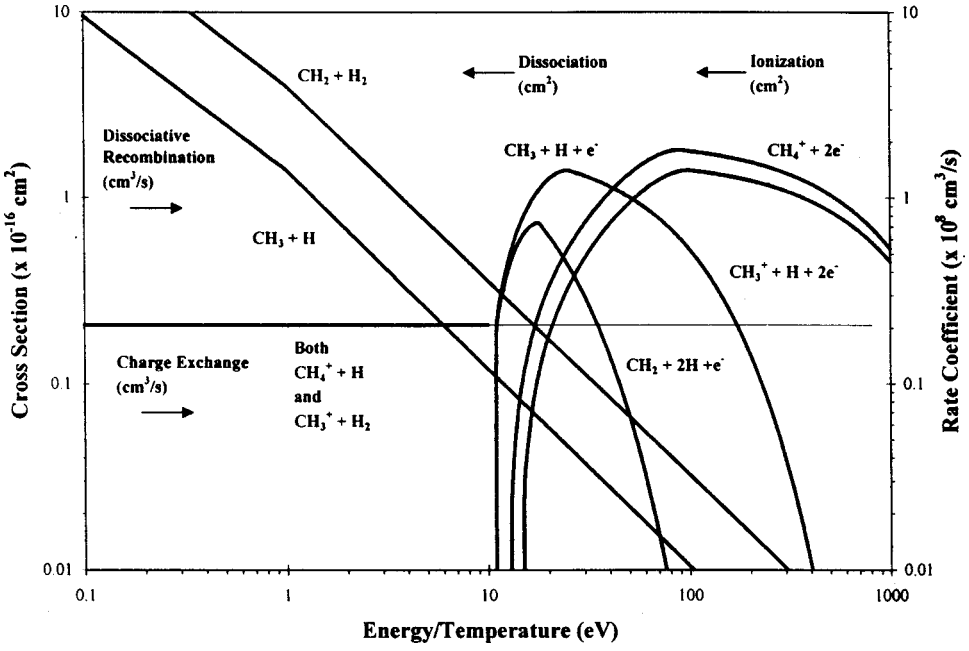

FIG. 4. Complete energy-dependent cross sections and rate coefficients for methane. Each plot is labeled by the products given off in the named reaction with a methane molecule (or ion in the case of recombination). One value for the rate coefficient for charge exchange is assumed constant (the horizontal line) since this value is valid in the temperature range of interest. Cross sections are given for dissociation and ionization, while rate coefficients are plotted for recombination and charge exchange.

Downloaded 21 Nov 2007 to 130.126.32.13. Redistribution subject to AIP license or copyright; see http://pop.aip.org/pop/copyright.jsp

The decay constant, λ, appears to generally increase with H and decrease C. We can approximate unknown values with

$$\lambda = (-64.3739\,\text{eV})\text{C} + (35.3963\,\text{eV})\text{H} + 668.358\,\text{eV}. \quad (10)$$

The branching ratios were known for the CH_y family[2] and for three heavier hydrocarbons:[19] C_2H_6, C_2H_4, and C_2H_2. This later data can be applied to other heavier hydrocarbons where branching ratios are not known. In general, the ionization and dissociation to the H_2 channel was favored ($\sim$70%), followed by the straight ionization ($\sim$20%). Ionization and dissociation to H was the least favored ($\sim$10%).

Table V summarizes the results when these approximations are used. Note that all energies are in electron volts and cross sections are in square centimeters. Also, for all energies below the threshold energy, the cross section is zero.

V. ELECTRON IMPACT DISSOCIATION

Plots of $\sigma(E)$ vs E for electron impact dissociation have the same general shape as those for electron impact ionization. Therefore, the same functional form was used to describe the cross-section curve in terms of four parameters: E_{th}, $E_{\max}$, $\sigma_{\max}$, and λ,

$$\sigma(E) = 0 \quad \text{for } E < E_{\text{th}}, \quad (11a)$$

$$\sigma(E) = \sigma_{\max}\left[1 - \frac{(E_{\max} - E)^2}{(E_{\max} - E_{\text{th}})^2}\right] \quad \text{for } E_{\text{th}} < E < E_{\max}, \quad (11b)$$

$$\sigma(E) = \sigma_{\max} \exp\left[\frac{-(E - E_{\max})}{\lambda}\right] \quad \text{for } E > E_{\max}. \quad (11c)$$

E_{th} is the threshold energy for dissociation and is always $\sim$10 eV. $E_{\max}$ is the energy at which the maximum value of the cross section, $\sigma_{\max}$, occurs. Finally, λ is a constant that determines the rate of decay of the cross section beyond $E_{\max}$.

In the case of electron impact dissociation, the only data available are for the CH_y family.[2,6] These known cross sections can be parameterized as shown in Table VI. This information is then used to make an extension to the heavier hydrocarbons. This is done by using the same graph shape, i.e., values of E_{th}, $E_{\max}$, and λ, as for the methane family but scaling the graph up and down with different values of $\sigma_{\max}$. A scaling law like the one used in (9) for electron impact ionization is again developed to accomplish this. Therefore, the scaling with the number of carbon and hydrogen atoms is the same as with ionization. However, here the maximum of the dissociation cross sections is generally only 80% of the maximum cross section for ionization,

$$\sigma_{\max} = (1.89\text{C} + 0.330\text{H} - 0.505) \times 10^{-16}\,\text{cm}^2. \quad (12)$$

From the CH_y family, the reactions are known to favor the dissociation of only one hydrogen rather than two by a 2:1 ratio. This branching ratio is used throughout the higher hydrocarbons. The resulting cross sections are shown in Table VII.

VI. HYDROCARBON TRANSPORT CALCULATIONS

To illustrate the use of these hydrocarbon reaction estimates, a series of calculations for the transport of chemically sputtered material from a tokamak carbon divertor surface have been performed. This was done using the WBC Monte Carlo impurity transport code[20] applied to the Joint European Torus (JET) MARK II carbon inner divertor. For the JET analysis, the complete set of hydrocarbon reactions and temperature-dependent rate coefficients discussed previously were implemented in WBC. This contrasts with earlier work,[9] for a very low temperature plasma in DIII-D, which did not incorporate the electron impact ionization processes.

A critical question which this modeling hopes to address is why much of the tritium (and deuterium) used in many JET shots is not pumped out at the end of the shot but instead appears to be trapped in deposited carbon layers in the plenum region near the inner divertor plate, apparently by the H/C codeposition process.[21] Our initial aim for this analysis is to compute general erosion/redeposition characteristics for the chemically sputtered carbon, including the percentage of sputtered carbon that reaches the plenum region.

The code was run for a deuterium plasma with three different spatially invariant near surface ($\sim$0–10 cm from the plate) plasma temperatures, $T_e = T_i = 1,3,10$ eV. These correspond roughly to the range estimated for various types of JET discharges. For comparison purposes in evaluating the effect of plasma temperature we used a fixed plasma density of 2×10^{20} m^{-3}. Other conditions include plasma sound-speed flow and debye/magnetic-type sheath condition. For each temperature case the code launches 10 000 hydrocarbons from the innermost divertor tile (''Tile 4'' of Fig. 2, Ref. 21). The hydrocarbons are launched as CH_4, C_2H_2, C_2H_4, C_2H_6, and C_3H_6, as discussed further in Ref. 9, and in proportions according to data from the UTIAS (Univeristy of Toronto Institute for Aerospace Studies) device.[22] The particles are launched with a thermal distribution corresponding to a 200 °C surface temperature. Particles then undergo elastic and inelastic collisions with the background plasma ions and electrons, and are subject to Lorentz force motion due to the tokamak magnetic field, and sheath electric field.

The hydrocarbon reactions are implemented in WBC using standard Monte Carlo methods. For a given particle in a given time interval the code determines whether a reaction occurs, and if so, what reaction, based on the probability determined by the applicable rate coefficients and the proton and electron density. The code follows each particle and resulting fragments until: (a) the particle leaves the near-surface region (including entering the plenum), or (b) the particle is redeposited on the divertor surface.

Table VIII summarizes code results in terms of several global redeposition parameters. Figure 2 shows the species mix of redeposited particles. Figure 3 shows the density profile of CD_2 molecules in the plasma. As shown in these results there is a substantial difference in hydrocarbon transport over the temperature range studied. Simpler models do not predict such dramatic differences. In general, proton impact ionization and electron recombination dominate at low

Downloaded 21 Nov 2007 to 130.126.32.13. Redistribution subject to AIP license or copyright; see http://pop.aip.org/pop/copyright.jsp

temperatures, and electron impact ionization dominates at higher temperatures. Hydrocarbon penetration into the plasma—as shown in Fig. 3 (and where trends are similar for the other hydrocarbons)—is greater at low temperatures. Although overall redeposition is always high, there is three times as much material lost (not-locally redeposited) at 1 eV than at 10 eV. Also, a much higher neutral fraction is redeposited at low temperatures. A related major difference is that at 1 eV about 10% of sputtered carbon goes to the louver region versus less than 1 % at 10 eV. Since lower temperatures prevailed in JET near the inner plate versus the outer plate during the campaign in question,[21] this result tends to explain the observed asymmetry in carbon deposition, namely being much more on the inner louver than the outer. Future work is planned on this subject with a focus on quantitative comparisons to carbon codeposition data using chemical sputtering yield estimates and more detailed plasma profiles.

VII. CONCLUSION

Although the values estimated herein are not calculated from first principles, reasoned physics was used to guide the approximations. This work attempts to include all available data and not leave out any important reactions. The final result is a complete set of cross sections or rate coefficients, as shown in Fig. 4 for methane, that can then be used in computer simulations to track hydrocarbon impurities in hydrogen plasmas. Using this data set, important issues such as asymmetries in JET's carbon redeposition can be examined whereas simpler hydrocarbon models would not be adequate. The model is presented here for wider consumption and as a challenge to the theoretical and experimental plasma physics community to further define these rates.

ACKNOWLEDGMENTS

The authors would like to thank Dr. David R. Schultz (ORNL) for his valuable suggestions and comments. This work was supported by the U.S. Department of Energy (DOE) and the National Science Foundation under DOE/NSF Contract No. DE-FG02-97ER54440, DOE/ALPS Contract No. DE-FG02-99ER54515, and ANL Contract No. 980332401.

[1] H. Tawara, in *Atomic and Molecular Processes in Fusion Edge Plasmas*, edited by R. K. Janev (Plenum, New York, 1995), pp. 461–496.
[2] A. B. Ehrhardt and W. D. Langer, Collisional Processes of Hydrocarbons in Hydrogen Plasmas, PPPL-2477 (1987). See National Technical Information Service Document No. DE88003462. Copies may be ordered from The National Technical Information Service, Springfield, VA.
[3] H. Abouelaziz, J. C. Gomet, D. Pasquerault, B. R. Rowe, and J. B. A. Mitchell, J. Chem. Phys. **99**, 237 (1993).
[4] J. B. A. Mitchell and C. Rebrion-Rowe, Int. Rev. Phys. Chem. **16**, 201 (1997).
[5] W. Hwang, Y.-K. Kim, and M. E. Rudd, J. Chem. Phys. **104**, 2956 (1996).
[6] T. Nakano, H. Toyoda, and H. Sugai, Jpn. J. Appl. Phys., Part 1 **30**, 2912 (1991).
[7] D. A. Alman and D. N. Ruzic, to be published in J. Nucl. Mater.
[8] D. A. Alman, M.S. thesis, University of Illinois (2000).
[9] J. N. Brooks, D. A. Alman, G. Federici, D. N. Ruzic, and D. G. White, J. Nucl. Mater. **266–269**, 58 (1999).
[10] J. N. Brooks, Z. Wang, D. N. Ruzic, and D. A. Alman, Hydrocarbon Rate Coefficients for Proton and Electron Impact Ionization, Dissociation, and Recombination in a Hydrogen Plasma, ANL/FPP/TM-297 (1999). See National Technical Information Service Document No. DE00012063. Copies may be ordered from The National Technical Information Service, Springfield, VA.
[11] E. W. McDaniel, V. Cermák, A. Dalgarno, E. E. Ferguson, and L. Friedman, *Ion–Molecule Reactions* (Wiley–Interscience, New York, 1970), pp. 293–296.
[12] R. C. Weast, *CRC Handbook of Chemistry and Physics* (CRC Press, Boca Raton, FL, 1985).
[13] A. A. Maryott and F. Buckley, *Table of Dielectric Constants and Electric Dipole Moments of Substances in the Gaseous State* (U.S. Bureau of Standards, Washington, DC, 1953).
[14] V. G. Anicich and W. T. Huntress, Jr., Astrophys. J., Suppl. Ser. **62**, 553 (1986).
[15] S. Dheandhanoo, R. Johnsen, and M. A. Biondi, Planet. Space Sci. **32**, 1301 (1984).
[16] G. I. Mackay, H. I. Schiff, and D. K. Bohme, Can. J. Chem. **59**, 1771 (1981).
[17] D. R. Schultz (private communication, 1988).
[18] P. M. Mul and J. W. McGowan, Astrophys. J. **237**, 749 (1980).
[19] H. Chatham, D. Hils, R. Robertson, and A. Gallagher, J. Chem. Phys. **81**, 1770 (1984).
[20] J. N. Brooks, Phys. Fluids B **8**, 1858 (1990).
[21] A. T. Peacock, P. Andrew, P. Cetier, J. P. Coad, G. Federici, F. H. Hurd, M. A. Pick, and C. H. Wu, J. Nucl. Mater. **266–269**, 423 (1999).
[22] B. V. Mech, A. A. Haasz, and J. W. Davis, J. Nucl. Mater. **241–243**, 1147 (1997).
[23] P. H. Rebut, R. J. Bickerton, and B. E. Keen, Nucl. Fusion **25**, 1011 (1985).

Downloaded 21 Nov 2007 to 130.126.32.13. Redistribution subject to AIP license or copyright; see http://pop.aip.org/pop/copyright.jsp